Published in final edited form as:
Proteins. 2008 August 15; 72(3): 1096–1103. doi:10.1002/prot.22095.

Crystal structure of a putative lysostaphin peptidase from *Vibrio cholerae*

Sugadev Ragumani[1], **Desigan Kumaran**[1], **Stephen K. Burley**[2], and **Subramanyam Swaminathan**[1,*]

[1]Biology Department, Brookhaven National Laboratory, Upton, New York 11973

[2]SGX Pharmaceuticals, Inc., San Diego, California 92121

Keywords

lysostaphin peptidase; LytM; glycyl-glycine or glycyl-alanine; latent form

INTRODUCTION

Peptidoglycan (PGN) constitutes the cell walls of virtually all bacteria, making it a target of the innate immune system.[1,2] PGN is a polymer of alternating β (1→ 4) linked *N*-acetylglucosamine (GlcNAc) and *N*-acetylmuramic acid (MurNAc), crossbridged by oligopeptide stems.[3–5] Lysostaphin type enzymes are believed to cleave the glycyl-glycine and glycyl-alanine bonds that occur in glycine-rich cross-bridges.[6,7] Lysostaphins represent potential anti staphylococcal agents. Specifically, they can eradicate *S. aureus* nasal colonization in the rat model and are effective in treating methicillin-resistant *S. aureus* endophthalmitis in rabbits.[8–10] These enzymes belong to metalloendopeptidase family and possess a conserved HXH active site motif. Together, D-Ala-D-Ala peptidase, the sonic hedgehog enzymes, the MepA-like enzymes, and the lysostaphine enzymes comprise the LAS enzyme superfamily.[11] Unlike other LAS enzymes the lyostaphins are synthesized as proenzymes and require proteolytic processing for activation.[12] To date, the only three-dimensional structure reported from the Lysostaphin type enzyme family is LytM from *Staphylococcus aureus*. Structures of both full length (residues 45–316; PDB ID: 1QWY) and truncated (residues 185–316; PDB ID: 2B44, 2BOP and 2B13) forms of LytM have been determined.[12,13] Cleavage of LytM between residues 45 and 185 removes Asn317, which blocks substrate access to the active site in the longer, inactive form of the enzyme.[12,13] The precise role(s) played by the lysostaphins in gram-negative bacteria remains unclear. In some gram-positive bacteria they participate in cell wall biogenesis.[11] Horizontal transfer of genes responsible for cell-wall polysaccharide synthesis is correlated with virulence of some strains of *Vibrio cholerae*, such as O139 Bengal,[14] suggesting that the cell-wall itself may represent a virulence factor. It is remarkable that *Vibrio cholerae* exerts its pathologic effects via a protein toxin on epithelial cells lining the small intestine that contains a modified form of GlcNAc.[15]

To better understand *V. cholerae* lysostaphin, the New York SGX Research Center for Structural Genomics (NYSGXRC; www.nysgxrc.org) targeted this protein (designated P01) for structure determination under the auspices of the National Institute of General Medical Sciences Protein Structure Initiative (PSI). We report the X-ray crystal structure of P01

*Correspondence to: S. Swaminathan, Biology Department, Brookhaven National Laboratory, Upton, NY 11973. swami@bnl.gov.

determined at 1.9-Å resolution. Comparison with extant structures of LytM from *S. aureus* permitted identification of the catalytic domain of P01 and elucidation of its mechanisms of activation and catalysis.

MATERIALS AND METHODS

Gene cloning and protein purification

The target gene (Gene ID 15640527) for the full-length putative peptidase from *Vibrio cholerae* (residues 63–412 and numbered as 4–353 in PDB ID 2GU1) was cloned into *E. coli* using primers CAACCTAAACGGATACACTA-TATG (forward) and CATGATCAAACTCTGATACTCG (reverse) in the pSGX (3) vector. The amplified gene was gel purified and cloned into TC - psb3 (TC) vector designed to express the protein of interest with a C-terminal hexa-histidine affinity tag (residues 356–361). Protein expression/purification utilized previously published protocols, which are described in detail in PepcDB (pepcdb.pdb.org).

Crystallization and data collection

Diffraction-quality crystals of native protein were obtained at room temperature via sitting drop vapor diffusion against a reservoir solution containing 0.1*M* Tris (pH8.5), 25% (w/v) PEG4000, and 0.2*M* ammonium sulfate (1 μL of reservoir solution plus 1 μL of protein solution at a concentration of 10 mg/mL). Crystals were flash frozen by direct immersion in liquid nitrogen using mother liquor supplemented with 15% (v/v) glycerol. Crystals belong to the monoclinic system in space group $P2_1$. Diffraction data from native crystals were obtained at 1.9-Å resolution using NSLS Beamline X29 (National Synchrotron Light Source, Brookhaven National Laboratory). The phase problem was overcome using mercurated crystals, generated by soaking in mother liquor supplemented with 2.5 m*M* $HgCl_2$ for 5 min. A two wavelength anomalous dispersion experiment was undertaken at 2.4-Å resolution under standard cryogenic conditions using NSLS Beamline X12C. Diffraction data were processed with HKL2000.[16] Crystal parameters and data collection statistics are provided in Table I.

Structure determination/refinement

The locations of two bound mercury atoms were obtained with SHELXD.[17] Phase refinement with SHARP[18] followed by density modification with SOLO-MON[19] yielded an electron density map adequate in quality for manual model building using O.[20] The final model was refined using CNS[21] and analyzed with PRO-CHECK[22] (Table I). Atomic coordinates and structure factor amplitudes have been deposited to the Protein Data Bank (PDB ID: 2GU1).

Overall structure/sequence

Figure 1 illustrates the structure of P01, which consists of three domains, designated I (residues 7–94, blue in Fig. 1), II (98–191, magenta in Fig. 1), and III (207–331, green/orange in Fig. 1). Domains I and II are similar in both amino acid sequence (60% similarity) and structure, with root-mean-square-deviation (r.m.s.d.) of 2.1 Å for 64 α-carbon atomic pairs comprising the common arrangement of a five-stranded, antiparallel β-sheet with a pair of α-helices buttressing one face (see Fig. 1). Domains II and III are connected by a small β-strand followed by a random coil segment (residues 190–206, red in Fig. 1), and the overall shape of the protomer is triangular. Domain III contains 11 antiparallel β-strands, four (β4 ↑ β5 ↓ β6 ↑ β10↓) of which are arranged from a platform supporting four loops [Loop 1 (residues 216–234 between β1 and β2); Loop 2 (260–263 between β4 and β5); Loop 3 (301–311, between β9 and β10); Loop 4 (319–321 between β10 and β11)] on its upper face.

Two β-strands (β3 and β9, orange in Fig. 1) are positioned on the lower face of the central β-sheet region.

A search using the DALI[23] server identified bacterial proteins that are structurally similar to Domain III of P01, including M23 from *Pseudomonas aeruginosa* (here-after designated P02) (PDB ID: 2HSI with *Z*-score = 16.6; sequence identity = 16% and r.m.s.d. = 0.9 Å for 99 α-carbon atomic pairs) and LytM lysostaphin metallo-protease from *S. aureus* (PDB ID: 2B13 with a *Z*-score = 15.4; sequence identity = 17% and r.m.s.d. = 2.0 Å for 119 α-carbon atomic pairs). The central core of six β-strands is common to all three structures, whereas the loop regions show more significant deviations (Figs. 2 and 3). Among the four loops, Loop 1 is the largest and shows the greatest deviations among P01, P02, and LytM. In P01, Loop 1 is stabilized by interactions with an N-terminal loop segment (residues 81–88). In full length LytM (PDB ID: 1QWY), Loop 1 is stabilized by analogous interactions with an N-terminal segment. In the truncated form of LytM (PDB ID: 2B13), Loop 1 interacts with Loop 2 and Loop 4 of an adjacent protomer in the crystal lattice. In contrast, Loop 1 of P02 appears disordered. In P01 and P02, Loops 2 and 4 face away from the β-core and interact with an N-terminal α-helix (residues 29–42 in P01 and 123–142 in P02). The orientation of the helix is essentially normal to the central β-sheet (see Fig. 4), burying nearly half the solvent accessible surface of the central beta core region. In the active form of LytM (PDB ID: 2B13) Loops 2 and 4 abut the β-core, where it helps to stabilize binding of a tri-glycine segment from an adjacent protomer in the crystal lattice.

A further 50 putative structural homologs of Domain III of P01 were identified with a PSI-BLAST search (*E*value $<2 \times 10^{-55}$, >36% identity). Most of these sequences are encoded by the genomes gram-negative bacteria, including a number of human pathogens such as *Shigella dysenteriae, Klebsiella pneumoniae, Salmonella typhimurium, Yersinia pestis*, and *Haemophilus influenzae* (see Fig. 3).

Notwithstanding the structure/sequence similarity of Domains I and II of P01, the DALI server detected only a single structural homolog of Domain I and nothing in the PDB similar to Domain II. Domain I resembles residues 46–177 of an outer membrane bacterial lipoprotein receptor LolB (PDB ID: 1IWM; *Z*-score = 5.3 with sequence identity = 8.0% and r.m.s.d. = 2.7 Å for 46 α-carbon atomic pairs).[24] LolB is an outer membrane receptor protein with eleven antiparallel β-strands and three α-helices. With the exception of residues 46–177, LolB does not resemble P01. PSI-BLAST was used to identify sequence-sequence matches with either α/β domain. Only a single match was detected, involving the entirety of Domain I and C-terminal residues 340–431 of Opacity-associated protein A (OpaA) from *H. influenzae* (*E*-value = 0.001 with sequence identity = 15%).[25] The OpaA protein belongs to the protein family pfam08525 and is annotated as a secreted protein. Shorter segments of Domain I showed sequence similarity to a fragment of ykuD from *B. subtilis* (residues 11–57 and 4–46, respectively, gave *E*-value = 0.0007 with sequence identity = 23%), both of which are similar in sequence to the LysM domain of *E. coli* membrane-bound lytic murein trans-glycosylase D.[26,27] The tertiary structures adopted by residues 11–57 of Domain I and by this same LysM domain are indeed similar to one another (PDB ID: 1E0G; with sequence identity = 25% and r.m.s.d. = 3.8 Å for 37 α-carbon atomic pairs).

P01 active site

An $|F_{observed}| - |F_{calculated}|$ difference Fourier synthe- sis of Domain III revealed an electron density feature with a bound metal ion in the β-core (see Fig. 5). Given the observed tetrahedral coordination geometry we modeled the metal ion as Zn^{21}, with interatomic distances to His 232 NE2 = 2.0 Å, Asp236 OD1 = 2.0 Å, and His313 ND1 = 2.1 Å. Both this arrangement of metal-chelating residues and their coordination geometry are strictly conserved among P01, P02, and the LytM. A residual electron density feature 1.94 Å from

the metal ion in the fourth coordination site was modeled as a water molecule (see Fig. 5). After the final refinement the B-factors for Zn and this water refined to 25.7 and 29.3 Å ^{2}, respectively. This entire arrangement is further stabilized by hydrogen bonds between the water molecule and His311 (O-NE2 = 2.8 Å) and between His311 and the main chain carbonyl oxygen atom of Gly309 (ND1-O = 2.7 Å). Most LAS enzymes possess an active site Zn^{21} ion, which is tetrahedrally coordinated to three protein sidechains (two His and an Asp) and a fourth ligand.[11] In the structures of D-Ala-D-Ala carboxypeptidase, VanX, and sonic hedgehog this fourth ligand is also a water molecule.[28–30] In the crystal structure of the active form of LytM, various anions such as phosphate, cacodylate, or tartrate occupy the fourth coordination site.[12] In the inactive form of LytM, an Asn sidechain serves as the fourth ligand water and is deemed responsible for enzyme autoinhibition.[13]

DISCUSSION

Domain III of P01 is a lysostaphin-type peptidase

The antiparallel β-core fold and the arrangement of conserved active site residues organized around a single divalent metal ion seen in Domain III of our structure of *V. cholerae* P01 are typical of LAS enzymes.[11] Closer examination of the structure of this domain reveals that P01 possesses two additional β-strands beneath the β-core and two highly conserved short motifs HXH (His311–His313) and HXXXD (His230–Asp234) making it a putative lysostaphin-type peptidase.[11] It is remarkable that our structure of P01 clearly shows the presence of a tightly-bound water molecule in the fourth metal ion coordination site, which has not been seen previously for any lysostaphin type peptidase. (Although a water molecule was never observed in the LytM active site, the proposed catalytic mechanism for this enzyme does invoke a nucleophilic water.[11,13])

Our structure of P01 shows a water molecule that is both coordinated to the active site Zn^{21} ion hydrogen bonded to the first His of the conserved HXH motif. Such an interaction suggests that the free electron pair of NE2 atom of His311 polarizes the water molecule, thereby activating the nucleophilic. ND1 of His311 is hydrogen bonded to the main chain carbonyl oxygen atom of Gly309, which would facilitate activation of the nucleophilic water (the general base). Our structural studies of P01, therefore, provide important new evidence supporting previously published predictions regarding the mechanism of action of LytM and other lysostaphin enzymes.[30,31]

Regulation of P01 enzyme activity

Comparison of the structures of the active and autoinhibited forms of LytM suggest that the longer form of the enzyme is rendered inactivate by the presence of an N-terminal segment that directs the sidechain of an Asn residue into the enzyme active site where it occupies the fourth metal ion coordination site. Once this segment of the polypeptide chain is removed, the enzyme is thought to bind a nucleophilic water molecule in the fourth coordination site and, thereby, support general acid-base catalysis. Although the presence of various anions in the crystals of activated LytM appear to preclude binding of the catalytic water molecule, the structure of this truncated form of LytM fortuitously demonstrated active site binding of a Gly-Gly-Gly tripeptide segment originating from an adjacent protomer in the crystal lattice.[12] This observation allows us to make a specific prediction regarding regulation of P01 enzyme activity.

The following analysis assumes that full-length P01 like LytM and other lysostaphin enzymes is not catalytically active. Our structure of full-length P01 provides evidence for a mechanism of autoinhibition distinct from that described for LytM. In P01, an α-helical segment (residues 28–42; blue in Fig. 4) occupies a portion of the β-core immediately

adjacent to the glycine tripeptide binding (putative substrate) site detected in LytM.[12] We suggest, therefore, that P01 is autoinhibited by this N-terminal α-helix *via* interference with substrate access to the active site. Strong, albeit indirect, support for this hypothesis comes from two sources.

First, given that LytM activation involves cleavage within the polypeptide chain N-terminal to the catalytic domain,[13] the amino acid sequence of P01 was submitted to Signal IP3.0 server to predict the possible signal peptides and cleavage sites.[33,34] This software predicted a maximum cleavage site score at Ile31, which falls within the first turn of the α-helix that appears to block substrate access to the β-core region of the enzyme. Second, we made structure-structure and sequence-sequence comparisons of P01 with other lysostaphin enzymes. Examination of the structure of P02 revealed the presence of an N-terminal α-helix (residues 123–142) that binds to the β-core region in the vicinity of Loops 2 and 4. Further enzyme kinetic studies beyond the scope of the PSI with various truncated forms of P01 will be required to fully confirm or refute our hypothesis regarding P01 autoinhibition.

Functional role of domain I

Domain I is similar in amino acid sequence to the C-terminal portion of the *H. influenzae* OpaA protein, which mediates binding of the bacterium to human conjunctival epithelial cells.[32] We do not currently know whether or not the C-terminal region of OpaA is involved in the binding to human conjunctival epithelial cells, but the presence of a LysM-like structural motif in Domain I suggests that it may bind PGN. The LysM sequence motif is found in many enzymes involved in cell wall degradation and is also present proteins associated with bacterial cell walls.[26] Further studies beyond the scope of the PSI will be required to establish what role, if any, Domain I plays in *V. cholereae* recognition of PGN present in human small intestinal epithelial cells.

Acknowledgments

Grant sponsor: National Institute of General Medical Sciences; Grant number: DEAC02-98CH10886; Grant sponsors: Biological and Environmental Research, Basic Energy Science (DOE), National Centre for Research Resources (NIH); Grant sponsor: US Department of Energy, Office of Science, Office of Basic Energy Sciences; Grant number: W-31-109-Eng-38.

The authors gratefully acknowledge data collection support from beamlines X12C (NSLS), X29A (NSLS), and SGX-CAT (31-1D; APS). Use of the SGX collaborative Access Team (SGX-CAT) beamline facilities at sector 31 of the Advanced Photon Source (APS) was provided by SGX pharmaceuticals, Inc., who constructed and operates the facility.

References

1. Hoffmann JA. The immune response of Drosophila. Nature. 2003; 426:33–38. [PubMed: 14603309]
2. Medzhitov R, Janeway CA Jr. Decoding the patterns of self and nonself by the innate immune system. Science. 2002; 296:298–300. [PubMed: 11951031]
3. Doyle, RJ.; Dziarski, R. The bacterial cell: peptidoglycan. In: Sussman, M., editor. Molecular medical microbiology. Vol. 1. 2001. p. 137-153.
4. van Heijenoort J. Formation of the glycan chains in the synthesis of bacterial peptidoglycan. Glycobiology. 2001; 11:25R–36R.
5. Stewart-Tull DE. Major component of the cell wall in gram positive organisms. Consists of a glycan backbone with alternating b 1–4 linked residues of N-acetyl-D-glucosamine and muramic acid. The immunological activities of bacterial peptidoglycans. Ann Rev Microbiol. 1980; 34:311. [PubMed: 7002027]
6. Ramadurai L, Lockwood KJ, Nadakavukaren MJ, Jayaswal RK. Characterization of a chromosomally encoded glycylglycine endo-peptidase of *Staphylococcus aureus*. Microbiology. 1999; 145 (Part 4):801–808. [PubMed: 10220159]

7. Sugai M, Fujiwara T, Akiyama T, Ohara M, Komatsuzawa H, Inoue S, Suginaka H. Purification and molecular characterization of glycylglycine endopeptidase produced by *Staphylococcus capitis* EPK1. J Bacteriol. 1997; 179:1193–1202. [PubMed: 9023202]
8. Kokai-Kun JF, Walsh SM, Chanturiya T, Mond JJ. Lysostaphin cream eradicates *Staphylococcus aureus* nasal colonization in a cotton rat model. Antimicrob Agents Chemother. 2003; 47:1589–1597. [PubMed: 12709327]
9. Dajcs JJ, Thibodeaux BA, Girgis DO, Shaffer MD, Delvisco SM, O'Callaghan RJ. Immunity to lysostaphin and its therapeutic value for ocular MRSA infections in the rabbit. Invest Ophthalmol Vis Sci. 2002; 43:3712–3716. [PubMed: 12454041]
10. Dajcs JJ, Thibodeaux BA, Hume EB, Zheng X, Sloop GD, O'Callaghan RJ. Lysostaphin is effective in treating methicillin-resistant *Staphylococcus aureus* endophthalmitis in the rabbit. Curr Eye Res. 2001; 22:451–457. [PubMed: 11584345]
11. Bochtler M, Odintsov SG, Marcyjaniak M, Sabala I. Similar active sites in lysostaphins and D-Ala-D-Ala metallopeptidases. Protein Sci. 2004; 13:854–861. [PubMed: 15044722]
12. Firczuk M, Mucha A, Bochtler M. Crystal structures of active LytM. J Mol Biol. 2005; 354:578–590. [PubMed: 16269153]
13. Odintsov SG, Sabala I, Marcyjaniak M, Bochtler M. Latent LytM at 1. 3A resolution. J Mol Biol. 2004; 335:775–785. [PubMed: 14687573]
14. Mooi FR, Bik EM. The evolution of epidemic *Vibrio cholerae* strains. Trends Microbiol. 1997; 5:161–165. [PubMed: 9141191]
15. Finne J, Breimer ME, Hansson GC, Karlsson KA, Leffler H, Vliegenthart JF, van Halbeek H. Novel polyfucosylated N-linked glycopeptides with blood group A H, X, and Y determinants from human small intestinal epithelial cells. J Biol Chem. 1989; 264:5720–5735. [PubMed: 2466830]
16. Otwinowski ZM, Minor W. Processing of X-ray diffraction data collected in oscillation mode. Methods Enzymol. 1997; 276:307–326.
17. Uson I, Sheldrick GM. Advances in direct methods for protein crystallography. Curr Opin Struct Biol. 1999; 9:643–648. [PubMed: 10508770]
18. Fortelle EDL, Bricogne G. Maximum-likelihood heavy atom parameter refinement in the MIR and MAD methods. Methods Enzymol. 1997; 276:472–493.
19. CCP4. Programs for protein crystallography. Acta Crystallogr D. 1994; 50:760–763. [PubMed: 15299374]
20. Jones TA, Zou JY, Cowan SW, Kjeldgaard M. Improved methods for the building of protein models in electron density maps and the location of errors in these models. Acta Crystallogr A. 1991; A47:110–119. [PubMed: 2025413]
21. Brunger AT, Adams PD, Clore GM, DeLano WL, Gros P, Grosse-Kunstleve RW, Jiang JS, Kuszewski J, Nilges M, Pannu NS, Read RJ, Rice LM, Simonson T, Warren GL. Crystallography and NMR system: a new software suite for macromolecular structure determination. Acta Crystallogr D Biol Crystallogr. 1998; 54 (Part 5):905–921. [PubMed: 9757107]
22. Laskowski RA, MacArthur MW, Moss DS, Thornton JM. PRO-CHECK: a program to check the stereochemical quality of protein structures. J Appl Crystallogr. 1993; 26:283–291.
23. Holm L, Sander C. Dali: a network tool for protein structure comparison. Trends Biochem Sci. 1995; 20:478–480. [PubMed: 8578593]
24. Takeda K, Miyatake H, Yokota N, Matsuyama S, Tokuda H, Miki K. Crystal structures of bacterial lipoprotein localization factors Lol A and Lol B. EMBO J. 2003; 22:3199–3209. [PubMed: 12839983]
25. Weiser JN, Chong ST, Greenberg D, Fong W. Identification and characterization of a cell envelope protein of *Haemophilus influenzae* contributing to phase variation in colony opacity and nasopharyngeal colonization. Mol Microbiol. 1995; 17:555–564. [PubMed: 8559074]
26. Bateman A, Bycroft M. The structure of a LysM domain from *E. coli* membrane-bound lytic murein transglycosylase D (MltD). J Mol Biol. 2000; 299:1113–1119. [PubMed: 10843862]
27. Bielnicki J, Devedjiev Y, Derewenda U, Dauter Z, Joachimiak A, Derewenda ZS. *B. subtilis* ykuD protein at 2. 0-Å resolution: insights into the structure and function of a novel, ubiquitous family of bacterial enzymes. Proteins. 2006; 62:144–151. [PubMed: 16287140]

28. Dideberg O, Charlier P, Dive G, Joris B, Frere JM, Ghuysen JM. Structure of a Zn^{21}-containing D-alanyl-D-alanine-cleaving carboxy-peptidase at 2. 5-Å resolution. Nature. 1982; 299:469–470. [PubMed: 7121588]

29. Hall TM, Porter JA, Beachy PA, Leahy DJ. A potential catalytic site revealed by the 1. 7-Å crystal structure of the amino-terminal signalling domain of Sonic hedgehog. Nature. 1995; 378:212–216. [PubMed: 7477329]

30. Bussiere DE, Pratt SD, Katz L, Severin JM, Holzman T, Park CH. The structure of VanX reveals a novel amino-dipeptidase involved in mediating transposon-based vancomycin resistance. Mol Cell. 1998; 2:75–84. [PubMed: 9702193]

31. Lessard IA, Walsh CT. VanX, a bacterial D-alanyl-D-alanine dipeptidase: resistance, immunity, or survival function? Proc Natl Acad Sci USA. 1999; 96:11028–11032. [PubMed: 10500118]

32. Prasadarao NV, Lysenko E, Wass CA, Kim KS, Weiser JN. Opacity-associated protein A contributes to the binding of *Haemophilus influenzae* to change epithelial cells. Infect Immun. 1999; 67:4153–4160. [PubMed: 10417187]

33. Nielsen H, Engelbrecht J, Brunak S, von Heijne G. Identification of prokaryotic and eukaryotic signal peptides and prediction of their cleavage sites. Protein Eng. 1997; 10:1–6. [PubMed: 9051728]

34. Nielsen H, Engelbrecht J, Brunak S, von Heijne G. A neural network method for identification of prokaryotic and eukaryotic signal peptides and prediction of their cleavage sites. Int J Neural Syst. 1997; 8:581–599. [PubMed: 10065837]

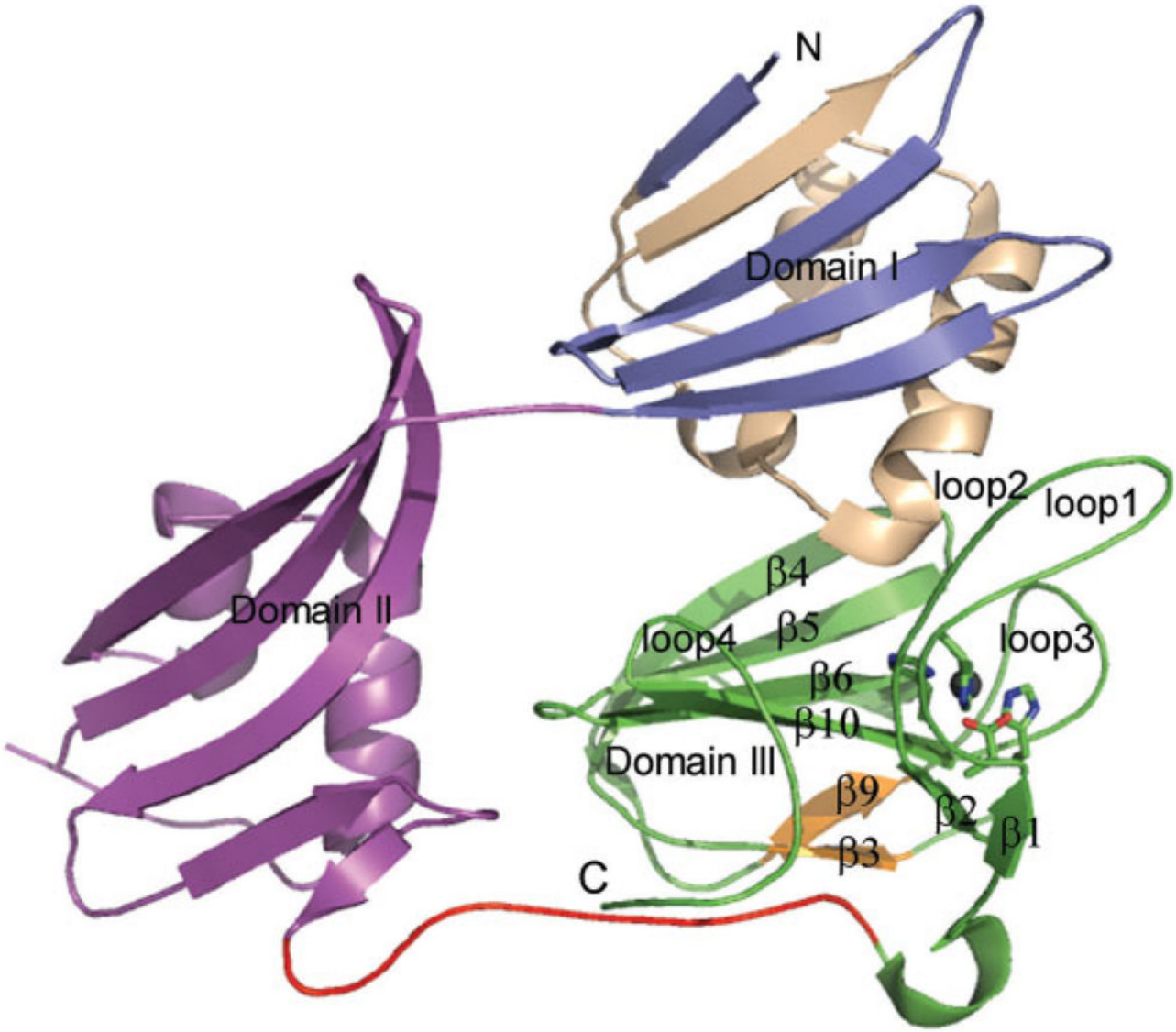

Figure 1.
Ribbons representation of putative lysostaphin peptidase from Vibrio cholerae. The three structural domains are labeled. N-terminal residues (11–57) of Domain I resembling LysM structural motif are shown in wheat color. In Domain III, strands β3 and β9 which are insertions to lysostaphin type peptidase are shown in orange. The active site residues and the zinc ion are shown as stick and ball model, respectively. The long loop connecting the N and C domains is shown in red.

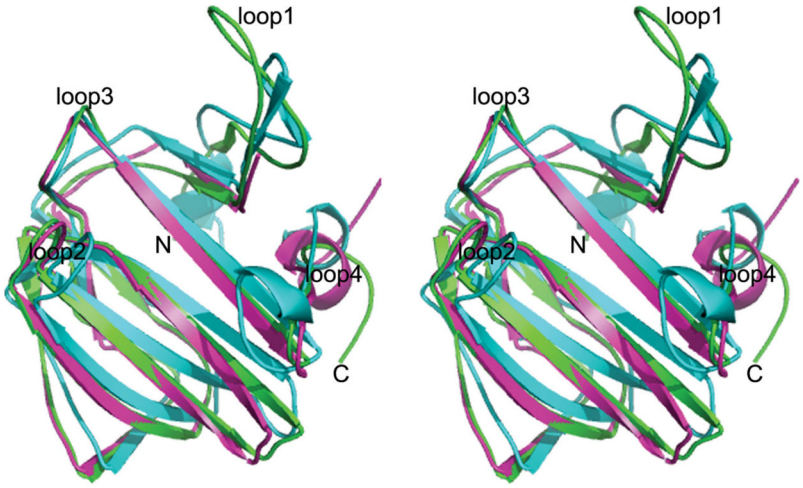

Figure 2.
Stereoview of C-terminal domains of P01, P02 and active LytM superimposed. P01, P02, and LytM are shown in green, purple and cyan, respectively. Loops 2 and 4 of LytM move toward the central β-core region compared to P01 and P02.

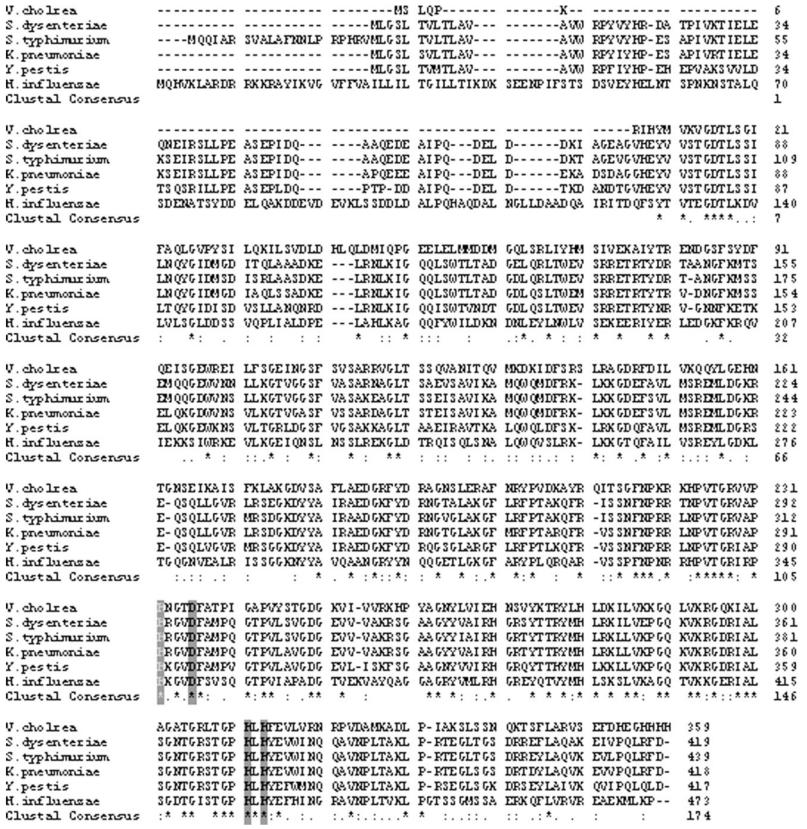

Figure 3.

Sequence alignment of putative peptidase from Vibrio cholerae (P01) homologs in human pathogenic bacteria like Shigella dysenteriae (GI:82776442), Klebsiella pneumoniae (GI: 152970918), Salmonella typhimurium (GI:16765232), Yersinia pestis (GI:16122301), Haemophilus influenzae (GI:145636322). The conserved residues are shown in “*”and the similar sequences are shown “.” The four conserved active site residues are highlighted in gray. N-terminal region of V. cholerae matches with other human pathogenic bacteria.

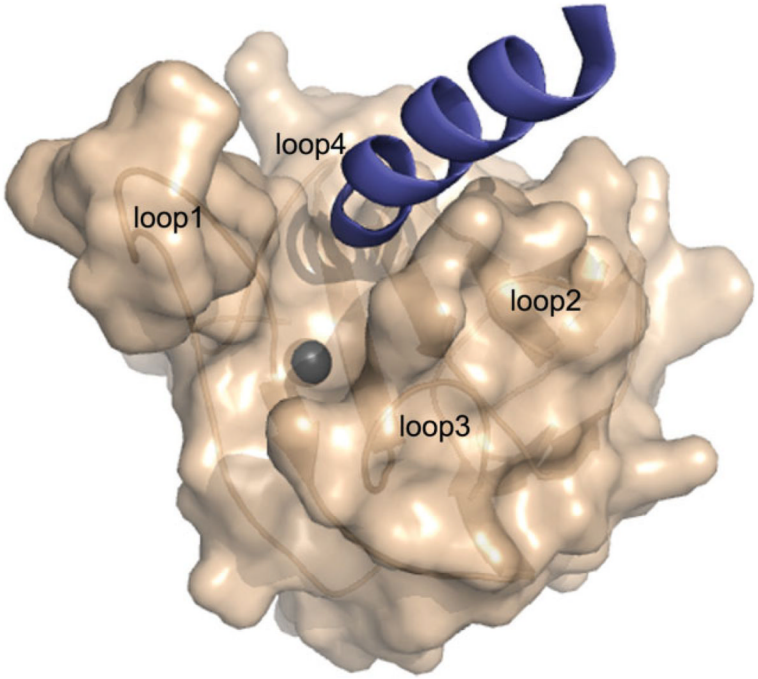

Figure 4.
A cartoon representation of N-terminal long α-helix (blue) and the surface representation of the C-terminal catalytic domain with the ribbons representation in laid (brown). The gray sphere represents Zn^{21} ion.

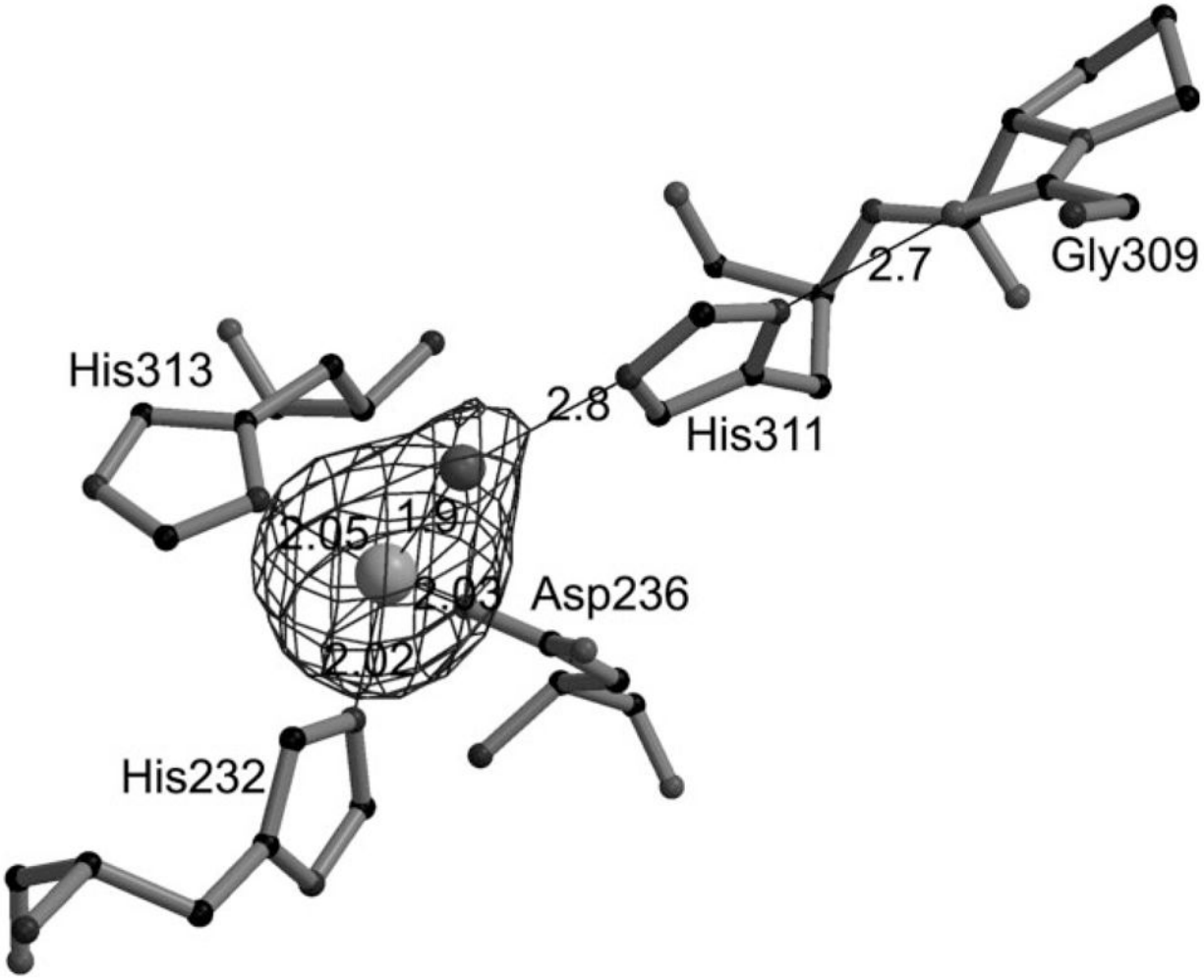

Figure 5.
C-terminal domain active site residues are shown in ball and stick model. Contour represents Sigma weighted Fo-Fc map at 3.0 σ for Zn^{21} and catalytic water molecule. The dotted lines represent the interaction between the atoms and their distances are in Å unit.

Table I

Data Collection Phasing and Refinement

	Crystal I (Hg-DAD)		Crystal II (Refinement)
Data set	**Peak**	**Edge**	**Native**
Cell dimensions (Å)	*a* = 49.21		*a* = 49.38
	b = 85.14		*b* = 85.40
	c = 53.40		*c* = 53.40
	β = 112.88°		β = 112.96°
Space group	$P2_1$		P21
Data collection statistics			
Wavelength (Å)	1.0062	1.0091	0.9795
Resolution range (Å)	50.0–2.44	50.0–2.43	50.0–1.9
Outermost Shell (Å)	2.52–2.44	2.53–2.43	1.99–1.9
Unique reflections	15,080 (1316)	15,105 (1379)	31,988 (1652)
Completeness (%)	98.5 (97.4)		92.0 (52.0)
Mean $I/\sigma(I)$	23.5 (3)	99.1 (91.6)	6.7 (2)
Redundancy	6.9 (5.1)	16.7 (2.5)	4.5 (2.0)
R_{merge}[a]	0.043 (0.21)	6.6 (5.3)	0.14 (0.30)
Phasing statistics	0.516	0.044 (.22)	
Phasing power[b] (ano)	0.31/0.28	0.411	
FOM[c]: (centric/acentric)	0.91	0.21/0.29	
After density modification		0.90	
Refinement statistics			
No. of reflections (work)			28,741
No. of reflections (test)			1987
R_{factor}[d]/R_{free}[e]			0.23/0.26
Resolution range (Å)			32.9–1.9
R.M.S.D. bond lengths (Å)			0.006
R.M.S.D. bond angles (°)			1.5
⟨*B*-values⟩			
Main-chain ($Å^2$)			31.8
Sidechain ($Å^2$)			34.8
Number of			
non-H atoms			2553
heteroatoms			2
water molecules			133
Residues (%) in the φ-ψ plot			
Most favored/additionally allowed			89.7/9.9

Values for the highest resolution shell are given within parentheses.

[a] $R_{merge} = \Sigma\ |I_i - \langle I \rangle| / \Sigma\ |I_i|$ where I_i is the intensity of the ith measurement, and $\langle I \rangle I$ is the mean intensity for that reflection.

[b] Phasing power as defined in SHARP.

[c] FOM (Figure of merit) as defined in SHARP.

[d] $R_{factor} = \Sigma \parallel F_{obs}|$, where $|F_{obs}|$ and $|F_{calc}|$ are the calculated and observe structure factor amplitudes, respectively.

[e] R_{free} = as for R_{factor}, but for 5% of the total reflections chosen at random and omitted from refinement.